Eur. Phys. J. C 11, 35–50 (1999)
Digital Object Identifier (DOI) 10.1007/s100529900166

THE EUROPEAN PHYSICAL JOURNAL C

Measurement of dijet photoproduction at high transverse energies at HERA

The ZEUS Collaboration

J. Breitweg, S. Chekanov, M. Derrick, D. Krakauer, S. Magill, B. Musgrave, A. Pellegrino, J. Repond, R. Stanek, R. Yoshida
Argonne National Laboratory, Argonne, IL, USA [p]

M.C.K. Mattingly
Andrews University, Berrien Springs, MI, USA

G. Abbiendi, F. Anselmo, P. Antonioli, G. Bari, M. Basile, L. Bellagamba, D. Boscherini[1], A. Bruni, G. Bruni, G. Cara Romeo, G. Castellini[2], L. Cifarelli[3], F. Cindolo, A. Contin, N. Coppola, M. Corradi, S. De Pasquale, P. Giusti, G. Iacobucci[4], G. Laurenti, G. Levi, A. Margotti, T. Massam, R. Nania, F. Palmonari, A. Pesci, A. Polini, G. Sartorelli, Y. Zamora Garcia[5], A. Zichichi
University and INFN Bologna, Bologna, Italy [f]

C. Amelung, A. Bornheim, I. Brock, K. Coböken, J. Crittenden, R. Deffner, M. Eckert[6], H. Hartmann, K. Heinloth, L. Heinz[7], E. Hilger, H.-P. Jakob, A. Kappes, U.F. Katz, R. Kerger, E. Paul, M. Pfeiffer[8], J. Rautenberg, H. Schnurbusch, A. Stifutkin, J. Tandler, A. Weber, H. Wieber
Physikalisches Institut der Universität Bonn, Bonn, Germany [c]

D.S. Bailey, O. Barret, W.N. Cottingham, B. Foster[9], G.P. Heath, H.F. Heath, J.D. McFall, D. Piccioni, J. Scott, R.J. Tapper
H.H. Wills Physics Laboratory, University of Bristol, Bristol, UK [o]

M. Capua, A. Mastroberardino, M. Schioppa, G. Susinno
Calabria University, Physics Dept.and INFN, Cosenza, Italy [f]

H.Y. Jeoung, J.Y. Kim, J.H. Lee, I.T. Lim, K.J. Ma, M.Y. Pac[10]
Chonnam National University, Kwangju, Korea [h]

A. Caldwell, N. Cartiglia, Z. Jing, W. Liu, B. Mellado, J.A. Parsons, S. Ritz[11], R. Sacchi, S. Sampson, F. Sciulli, Q. Zhu[12]
Columbia University, Nevis Labs., Irvington on Hudson, N.Y., USA [q]

P. Borzemski, J. Chwastowski, A. Eskreys, J. Figiel, K. Klimek, K. Olkiewicz, M.B. Przybycień, L. Zawiejski
Inst. of Nuclear Physics, Cracow, Poland [j]

L. Adamczyk[13], B. Bednarek, K. Jeleń, D. Kisielewska, A.M. Kowal, T. Kowalski, M. Przybycień, E. Rulikowska-Zarębska, L. Suszycki, J. Zając
Faculty of Physics and Nuclear Techniques, Academy of Mining and Metallurgy, Cracow, Poland [j]

Z. Duliński, A. Kotański
Jagellonian Univ., Dept. of Physics, Cracow, Poland [k]

L.A.T. Bauerdick, U. Behrens, J.K. Bienlein, C. Burgard, K. Desler, G. Drews, A. Fox-Murphy, U. Fricke, F. Goebel, P. Göttlicher, R. Graciani, T. Haas, W. Hain, G.F. Hartner, D. Hasell[14], K. Hebbel, K.F. Johnson[15], M. Kasemann[16], W. Koch, U. Kötz, H. Kowalski, L. Lindemann, B. Löhr, M. Martínez, J. Milewski[17], M. Milite, T. Monteiro[18], M. Moritz, D. Notz, F. Pelucchi, K. Piotrzkowski, M. Rohde, P.R.B. Saull, A.A. Savin, U. Schneekloth, O. Schwarzer[19], F. Selonke, M. Sievers, S. Stonjek, E. Tassi, G. Wolf, U. Wollmer, C. Youngman, W. Zeuner
Deutsches Elektronen-Synchrotron DESY, Hamburg, Germany

B.D. Burow[20], C. Coldewey, H.J. Grabosch, A. Lopez-Duran Viani, A. Meyer, K. Mönig, S. Schlenstedt, P.B. Straub
DESY Zeuthen, Zeuthen, Germany

G. Barbagli, E. Gallo, P. Pelfer
University and INFN, Florence, Italy [f]

G. Maccarrone, L. Votano
INFN, Laboratori Nazionali di Frascati, Frascati, Italy [f]

A. Bamberger, S. Eisenhardt[21], P. Markun, H. Raach, S. Wölfle
Fakultät für Physik der Universität Freiburg i.Br., Freiburg i.Br., Germany [c]

N.H. Brook[22], P.J. Bussey, A.T. Doyle, S.W. Lee, N. Macdonald, G.J. McCance, D.H. Saxon, L.E. Sinclair, I.O. Skillicorn, E. Strickland, R. Waugh
Dept. of Physics and Astronomy, University of Glasgow, Glasgow, UK [o]

I. Bohnet, N. Gendner, U. Holm, A. Meyer-Larsen, H. Salehi, K. Wick
Hamburg University, I. Institute of Exp. Physics, Hamburg, Germany [c]

A. Garfagnini, I. Gialas[23], L.K. Gladilin[24], D. Kçira[25], R. Klanner, E. Lohrmann, G. Poelz, F. Zetsche
Hamburg University, II. Institute of Exp. Physics, Hamburg, Germany [c]

T.C. Bacon, J.E. Cole, G. Howell, L. Lamberti[26], K.R. Long, D.B. Miller, A. Prinias[27], J.K. Sedgbeer, D. Sideris, A.D. Tapper, R. Walker
Imperial College London, High Energy Nuclear Physics Group, London, UK [o]

U. Mallik, S.M. Wang
University of Iowa, Physics and Astronomy Dept., Iowa City, USA [p]

P. Cloth, D. Filges
Forschungszentrum Jülich, Institut für Kernphysik, Jülich, Germany

T. Ishii, M. Kuze, I. Suzuki[28], K. Tokushuku[29], S. Yamada, K. Yamauchi, Y. Yamazaki
Institute of Particle and Nuclear Studies, KEK, Tsukuba, Japan [g]

S.H. Ahn, S.H. An, S.J. Hong, S.B. Lee, S.W. Nam[30], S.K. Park
Korea University, Seoul, Korea [h]

H. Lim, I.H. Park, D. Son
Kyungpook National University, Taegu, Korea [h]

F. Barreiro, J.P. Fernández, G. García, C. Glasman[31], J.M. Hernández[32], L. Labarga, J. del Peso, J. Puga, I. Redondo[33], J. Terrón
Univer. Autónoma Madrid, Depto de Física Teórica, Madrid, Spain [n]

F. Corriveau, D.S. Hanna, J. Hartmann[34], W.N. Murray[6], A. Ochs, S. Padhi, M. Riveline, D.G. Stairs, M. St-Laurent, M. Wing
McGill University, Dept. of Physics, Montréal, Québec, Canada [a], [b]

T. Tsurugai
Meiji Gakuin University, Faculty of General Education, Yokohama, Japan

V. Bashkirov[35], B.A. Dolgoshein
Moscow Engineering Physics Institute, Moscow, Russia [l]

G.L. Bashindzhagyan, P.F. Ermolov, Yu.A. Golubkov, L.A. Khein, N.A. Korotkova, I.A. Korzhavina, V.A. Kuzmin, O.Yu. Lukina, A.S. Proskuryakov, L.M. Shcheglova[36], A.N. Solomin[36], S.A. Zotkin
Moscow State University, Institute of Nuclear Physics, Moscow, Russia [m]

C. Bokel, M. Botje, N. Brümmer, J. Engelen, E. Koffeman, P. Kooijman, A. van Sighem, H. Tiecke, N. Tuning, J.J. Velthuis, W. Verkerke, J. Vossebeld, L. Wiggers, E. de Wolf
NIKHEF and University of Amsterdam, Amsterdam, Netherlands [i]

D. Acosta[37], B. Bylsma, L.S. Durkin, J. Gilmore, C.M. Ginsburg, C.L. Kim, T.Y. Ling, P. Nylander
Ohio State University, Physics Department, Columbus, Ohio, USA [p]

H.E. Blaikley, S. Boogert, R.J. Cashmore[18], A.M. Cooper-Sarkar, R.C.E. Devenish, J.K. Edmonds, J. Große-Knetter[38], N. Harnew, T. Matsushita, V.A. Noyes[39], A. Quadt[18], O. Ruske, M.R. Sutton, R. Walczak, D.S. Waters
Department of Physics, University of Oxford, Oxford, UK [o]

A. Bertolin, R. Brugnera, R. Carlin, F. Dal Corso, S. Dondana, U. Dosselli, S. Dusini, S. Limentani, M. Morandin, M. Posocco, L. Stanco, R. Stroili, C. Voci
Dipartimento di Fisica dell' Università and INFN, Padova, Italy [f]

L. Iannotti[40], B.Y. Oh, J.R. Okrasiński, W.S. Toothacker, J.J. Whitmore
Pennsylvania State University, Dept. of Physics, University Park, PA, USA [q]

Y. Iga
Polytechnic University, Sagamihara, Japan [g]

G. D'Agostini, G. Marini, A. Nigro, M. Raso
Dipartimento di Fisica, Univ. 'La Sapienza' and INFN, Rome, Italy [f]

C. Cormack, J.C. Hart, N.A. McCubbin, T.P. Shah
Rutherford Appleton Laboratory, Chilton, Didcot, Oxon, UK [o]

D. Epperson, C. Heusch, H.F.-W. Sadrozinski, A. Seiden, R. Wichmann, D.C. Williams
University of California, Santa Cruz, CA, USA [p]

N. Pavel
Fachbereich Physik der Universität-Gesamthochschule Siegen, Germany [c]

H. Abramowicz[41], S. Dagan[42], S. Kananov[42], A. Kreisel, A. Levy[42], A. Schechter
Raymond and Beverly Sackler Faculty of Exact Sciences, School of Physics, Tel-Aviv University, Tel-Aviv, Israel [e]

T. Abe, T. Fusayasu, M. Inuzuka, K. Nagano, K. Umemori, T. Yamashita
Department of Physics, University of Tokyo, Tokyo, Japan [g]

R. Hamatsu, T. Hirose, K. Homma[43], S. Kitamura[44], T. Nishimura
Tokyo Metropolitan University, Dept. of Physics, Tokyo, Japan [g]

M. Arneodo[45], R. Cirio, M. Costa, M.I. Ferrero, S. Maselli, V. Monaco, C. Peroni, M.C. Petrucci, M. Ruspa, A. Solano, A. Staiano
Università di Torino, Dipartimento di Fisica Sperimentale and INFN, Torino, Italy [f]

M. Dardo
II Faculty of Sciences, Torino University and INFN - Alessandria, Italy [f]

D.C. Bailey, C.-P. Fagerstroem, R. Galea, T. Koop, G.M. Levman, J.F. Martin, R.S. Orr, S. Polenz, A. Sabetfakhri, D. Simmons
University of Toronto, Dept. of Physics, Toronto, Ont., Canada [a]

J.M. Butterworth, C.D. Catterall, M.E. Hayes, E.A. Heaphy, T.W. Jones, J.B. Lane
University College London, Physics and Astronomy Dept., London, UK [o]

J. Ciborowski, G. Grzelak[46], R.J. Nowak, J.M. Pawlak, R. Pawlak, B. Smalska, T. Tymieniecka, A.K. Wróblewski, J.A. Zakrzewski, A.F. Żarnecki
Warsaw University, Institute of Experimental Physics, Warsaw, Poland [j]

M. Adamus, T. Gadaj
Institute for Nuclear Studies, Warsaw, Poland [j]

O. Deppe, Y. Eisenberg[42], D. Hochman, U. Karshon[42]
Weizmann Institute, Department of Particle Physics, Rehovot, Israel [d]

W.F. Badgett, D. Chapin, R. Cross, C. Foudas, S. Mattingly, D.D. Reeder, W.H. Smith, A. Vaiciulis[47], T. Wildschek, M. Wodarczyk
University of Wisconsin, Dept. of Physics, Madison, WI, USA [p]

A. Deshpande, S. Dhawan, V.W. Hughes
Yale University, Department of Physics, New Haven, CT, USA [p]

S. Bhadra, W.R. Frisken, R. Hall-Wilton, M. Khakzad, S. Menary, W.B. Schmidke
York University, Dept. of Physics, Toronto, Ont., Canada [a]

[1] now visiting scientist at DESY
[2] also at IROE Florence, Italy
[3] now at Univ. of Salerno and INFN Napoli, Italy
[4] also at DESY
[5] supported by Worldlab, Lausanne, Switzerland
[6] now a self-employed consultant
[7] now at Spectral Design GmbH, Bremen
[8] now at EDS Electronic Data Systems GmbH, Troisdorf, Germany
[9] also at University of Hamburg, Alexander von Humboldt Research Award
[10] now at Dongshin University, Naju, Korea
[11] now at NASA Goddard Space Flight Center, Greenbelt, MD 20771, USA

[12] now at Greenway Trading LLC
[13] supported by the Polish State Committee for Scientific Research, grant No. 2P03B14912
[14] now at Massachusetts Institute of Technology, Cambridge, MA, USA
[15] visitor from Florida State University
[16] now at Fermilab, Batavia, IL, USA
[17] now at ATM, Warsaw, Poland
[18] now at CERN
[19] now at ESG, Munich
[20] now an independent researcher in computing
[21] now at University of Edinburgh, Edinburgh, UK
[22] PPARC Advanced fellow
[23] visitor of Univ. of Crete, Greece, partially supported by DAAD, Bonn - Kz. A/98/16764
[24] on leave from MSU, supported by the Fig, contract I-0444-176.07/95
[25] supported by DAAD, Bonn - Kz. A/98/12712
[26] supported by an EC fellowship
[27] PPARC Post-doctoral fellow
[28] now at Osaka Univ., Osaka, Japan
[29] also at University of Tokyo
[30] now at Wayne State University, Detroit
[31] supported by an EC fellowship number ERBFMBICT 972523
[32] now at HERA-B/DESY supported by an EC fellowship No.ERBFMBICT 982981
[33] supported by the Comunidad Autonoma de Madrid
[34] now at debis Systemhaus, Bonn, Germany
[35] now at Loma Linda University, Loma Linda, CA, USA
[36] partially supported by the Foundation for German-Russian Collaboration DFG-RFBR (grant no. 436 RUS 113/248/3 and no. 436 RUS 113/248/2)
[37] now at University of Florida, Gainesville, FL, USA
[38] supported by the Feodor Lynen Program of the Alexander von Humboldt foundation
[39] now with Physics World, Dirac House, Bristol, UK
[40] partly supported by Tel Aviv University
[41] an Alexander von Humboldt Fellow at University of Hamburg
[42] supported by a MINERVA Fellowship
[43] now at ICEPP, Univ. of Tokyo, Tokyo, Japan
[44] present address: Tokyo Metropolitan University of Health Sciences, Tokyo 116-8551, Japan
[45] now also at Università del Piemonte Orientale, 28100 Novara, Italy, and Alexander von Humboldt fellow at the University of Hamburg
[46] supported by the Polish State Committee for Scientific Research, grant No. 2P03B09308
[47] now at University of Rochester, Rochester, NY, USA

Received: 18 May 1999 / Published online: 14 October 1999

Abstract. The cross section for dijet photoproduction at high transverse energies is presented as a function of the transverse energies and the pseudorapidities of the jets. The measurement is performed using a sample of ep-interactions corresponding to an integrated luminosity of 6.3 pb^{-1}, recorded by the ZEUS detector. Jets are defined by applying a k_T-clustering algorithm to the hadrons observed in the final state. The measured cross sections are compared to next-to-leading order QCD calculations. In a kinematic regime where theoretical uncertainties are expected to be small, the measured cross sections are higher than these calculations.

[a] supported by the Natural Sciences and Engineering Research Council of Canada (NSERC)
[b] supported by the FCAR of Québec, Canada
[c] supported by the German Federal Ministry for Education and Science, Research and Technology (BMBF), under contract numbers 057BN19P, 057FR19P, 057HH19P, 057HH29P, 057SI75I
[d] supported by the MINERVA Gesellschaft für Forschung GmbH, the German Israeli Foundation, and by the Israel Ministry of Science
[e] supported by the German-Israeli Foundation, the Israel Science Foundation, the U.S.-Israel Binational Science Foundation, and by the Israel Ministry of Science
[f] supported by the Italian National Institute for Nuclear Physics (INFN)
[g] supported by the Japanese Ministry of Education, Science and Culture (the Monbusho) and its grants for Scientific Research
[h] supported by the Korean Ministry of Education and Korea Science and Engineering Foundation
[i] supported by the Netherlands Foundation for Research on Matter (FOM)

1 Introduction

In photoproduction at HERA a quasi real photon, emitted from the incoming positron, collides with the incoming proton. In leading order quantum chromodynamics (QCD), two processes contribute to the photoproduction of jets: the direct process, in which the photon couples directly to a parton in the proton, and the resolved process, in which the photon acts as a source of partons, one of which scatters from a parton in the proton. Beyond the leading order in QCD, direct and resolved processes are not distinctly separable.

The cross section for jet photoproduction is sensitive to the partonic structures of both the proton and the photon. In the kinematic regime of the measurement presented in this paper, the fractional momentum x at which partons inside the proton are probed lies predominantly in the region between 10^{-2} and 10^{-1}. At these x values the parton densities in the proton are strongly constrained by measurements of the structure function F_2^p in deep inelastic lepton-proton scattering [1]. The fractional momentum x_γ at which partons in the photon are probed lies between 0.1 and 1. For x_γ values above 0.5 the quark densities in the photon are not strongly constrained by F_2^γ data obtained from $\gamma\gamma^*$ scattering at e^+e^- experiments [2].

The investigation presented in this paper aims to constrain more tightly the parton densities in the photon at high x_γ, where the contribution from quarks dominates, by exploiting their influence on the dijet photoproduction cross section. For this purpose the dijet cross section is measured in a kinematic regime where next-to-leading order (NLO) QCD calculations are expected to describe the data. It should be noted here that jet measurements at the Tevatron [3], although generally in good agreement with NLO-QCD, show discrepancies in the comparison of the 630 GeV and 1800 GeV data sets. These may be connected to non-perturbative effects, such as a possible underlying event [4]. A number of these effects, which may also be of relevance to the present study, have been investigated in this paper.

This paper builds on the improved understanding of jet photoproduction and of comparisons to NLO-QCD calculations gained in previous analyses [5] - [10] and on a significant theoretical effort in the recent past [11] - [24]. Events with two or more high-transverse-energy jets are used, one of which is required to have transverse energy greater than 14 GeV and the second one greater than 11 GeV. A previous jet photoproduction analysis [8] has shown that for jets with transverse energy greater than 11 GeV, the dijet cross section agrees with NLO-QCD predictions, within the experimental uncertainties of that analysis.

2 Experimental setup

The data used in this paper were collected in 1995 with the ZEUS detector at HERA, colliding positrons at an energy of $E_e = 27.5$ GeV with protons at an energy of $E_p = 820$ GeV, yielding a total CM energy of $\sqrt{s} = \sqrt{4E_eE_p} \approx 300$ GeV. The data sample corresponds to an integrated luminosity of 6.3 pb^{-1}.

The ZEUS detector is described in detail elsewhere [25]. The main components used in this analysis are the uranium-scintillator calorimeter (CAL) and the central tracking detector (CTD). The CAL [25,26] covers 99.9% of the total solid angle and is subdivided into forward, barrel and rear parts, covering the pseudorapidity regions $4.3 \geq \eta > 1.1$, $1.1 \geq \eta > -0.75$ and $-0.75 \geq \eta > -3.8$, respectively[1]. Test beam measurements yield energy resolutions of $\sigma(E)/E = 18\%/\sqrt{E(\mathrm{GeV})}$ for electrons and $\sigma(E)/E = 35\%/\sqrt{E(\mathrm{GeV})}$ for hadrons [27]. The CTD [28] is a cylindrical drift chamber, situated in a 1.43 T solenoidal magnetic field, covering the polar angular region $15^\circ < \theta < 164^\circ$. The transverse momentum resolution for full-length tracks can be parametrised as $\sigma(p_T)/p_T = 0.0058p_T \oplus 0.0065 \oplus 0.0014/p_T$, with p_T in GeV. The luminosity collected by ZEUS is measured from the rate of the Bremsstrahlung process $e^+p \to e^+p\gamma$. A three-level trigger system is used to select events online [8,25].

3 Definition of the cross section

The relevant variables for the dijet cross section measurement presented in this paper are the following:

- the transverse energy, E_T^{jet}, the azimuthal angle, ϕ^{jet}, and the pseudorapidity, η^{jet}, of the jets;
- the scaled energy transfer from the positron to the proton in the proton's rest frame, defined as:

$$y = \frac{q \cdot p}{k \cdot p}\,,\ 0 < y < 1\,, \qquad (1)$$

[1] The ZEUS coordinate system is defined as right-handed with the Z axis pointing in the proton beam direction, hereafter referred to as forward, and the X axis horizontal, pointing towards the centre of HERA. The pseudorapidity is defined as $\eta = -\ln(\tan\frac{\theta}{2})$, where the polar angle θ is taken with respect to the proton beam direction

[j] supported by the Polish State Committee for Scientific Research, grant No. 115/E-343/SPUB/P03/154/98, 2P03B03216, 2P03B04616, 2P03B10412, 2P03B05315, 2P03B03517, and by the German Federal Ministry of Education and Science, Research and Technology (BMBF)
[k] supported by the Polish State Committee for Scientific Research (grant No. 2P03B08614 and 2P03B06116)
[l] partially supported by the German Federal Ministry for Education and Science, Research and Technology (BMBF)
[m] supported by the Fund for Fundamental Research of Russian Ministry for Science and Education and by the German Federal Ministry for Education and Science, Research and Technology (BMBF)
[n] supported by the Spanish Ministry of Education and Science through funds provided by CICYT
[o] supported by the Particle Physics and Astronomy Research Council
[p] supported by the US Department of Energy
[q] supported by the US National Science Foundation

where q, k and p are the four-momenta of the exchanged photon, the incoming positron and the incoming proton, respectively. Neglecting mass terms, y is related to the centre-of-mass energy in the photon-proton system, $W_{\gamma p} = \sqrt{ys}$. In the photoproduction regime, where the exchanged photon is almost real, y is equivalent to the fractional energy of the incoming positron carried by the photon;

– the fractional longitudinal momentum of the photon participating in the production of the two highest-transverse-energy jets, defined as [6]:

$$x_\gamma^{obs} = \frac{E_{T\,1}^{jet} e^{-\eta_1^{jet}} + E_{T\,2}^{jet} e^{-\eta_2^{jet}}}{2yE_e}\,, \qquad (2)$$

where $E_{T\,1,2}^{jet}$ and $\eta_{1,2}^{jet}$ are the transverse energies and the pseudorapidities of the two highest-transverse-energy jets;

– the virtuality of the exchanged photon:

$$Q^2 = -q^2\,. \qquad (3)$$

The cross section presented in this paper is compared to NLO-QCD predictions. It is restricted to a specific set of conditions, to minimise theoretical uncertainties.

– An asymmetric cut is applied on the transverse energy of the two highest-transverse-energy jets. The application of a symmetric cut poses a stability problem for some of the available NLO-QCD calculations [12,13].
– Symmetrisation of the cross section with respect to the pseudorapidity of the two highest-transverse-energy jets has been claimed to remove infrared instabilities in the NLO-QCD calculations [14]. This entails analysing each event twice, as explained below.
– Jets are defined using the longitudinally invariant k_T-clustering algorithm [15] in the inclusive mode [16], where the parameter R is chosen equal to 1. This algorithm provides a jet reconstruction that is suitable for comparisons between data and theory [17].

The dijet photoproduction cross section presented in this paper refers to events in which at least two jets, as defined by the k_T-clustering algorithm, are found in the hadronic final state. These jets are required to have pseudorapidities between -1 and 2, transverse energy of the highest-transverse-energy jet, $E_{T\,leading}^{jet}$, greater than 14 GeV and the transverse energy of the second-highest-transverse-energy jet, $E_{T\,second}^{jet}$, greater than 11 GeV. The cross section is given in the kinematic region defined by: $Q^2 < 1$ GeV^2 and $0.20 < y < 0.85$.

This cross section is measured as a function of three variables: $E_{T\,leading}^{jet}$, η_1^{jet} and η_2^{jet}. The cross section is symmetrised with respect to the pseudorapidities of the two jets. Every event contributes twice to the cross section, once with $\eta_1^{jet} = \eta_{leading}^{jet}$ and $\eta_2^{jet} = \eta_{second}^{jet}$ and a second time with $\eta_1^{jet} = \eta_{second}^{jet}$ and $\eta_2^{jet} = \eta_{leading}^{jet}$.

The cross section is determined for the full range of x_γ^{obs} values and for a direct-photoproduction-enriched region with $x_\gamma^{obs} > 0.75$. The cross section as a function of the pseudorapidity of the jets is also measured in a narrower band of y values between 0.50 and 0.85, where the sensitivity to the photon structure is expected to be higher, as will be explained in Sect. 9.2.

4 Comparisons to NLO-QCD

The measured cross sections are compared to NLO-QCD calculations by four different groups: P. Aurenche et al. [18], S. Frixione et al. [13,19], B. Harris et al. [20] and M. Klasen et al. [21]. These calculations differ in the handling of divergences [22,23].

All calculations use the CTEQ4M [29] parameterisation of the parton densities in the proton. The value of Λ_{QCD} is chosen to match that of this set of parton distribution functions. For the parton densities in the photon three parameterisations are used, GRV-HO [30,31], GS96-HO [32] and AFG-HO [33].

In all calculations the renormalisation and factorisation scales are chosen equal to the transverse energy of the highest-transverse-energy jet. The variation in the NLO-QCD calculations of the presented cross section has been found to be less than 15%, when the scales are varied between half and twice this value.

The NLO-QCD calculations do not include fragmentation. Jets are defined on the basis of the outgoing partons. While the momenta of jets at high transverse energies are expected to correspond closely to the momenta of the partons produced in the hard subprocess, the measured jet cross sections are affected at some level by the fragmentation. In a study using the HERWIG 5.9 and the PYTHIA 5.7 Monte Carlo photoproduction models, the dijet cross section for jets of hadrons was compared to that for partons produced in the two-to-two hard subprocess and in the parton showers which were grouped into "parton jets" using the k_T-clustering algorithm.

In HERWIG the change in the cross section due to the fragmentation was found to be less than 10% in most of the present kinematic region. However for events in which one jet has $\eta^{jet} < 0$ the cross section is reduced by more than 10% due to fragmentation and when both jets have $\eta^{jet} < 0$ the cross section is reduced by $\sim 40\%$. In PYTHIA the reduction of the cross section due to fragmentation is much smaller, but shows the same trend. In a related study, presented in reference [24], HERWIG 5.9 was used to compare the cross section for jets of hadrons to that for jets of partons, produced in the two-to-two hard subprocess. The relative difference between these cross sections was found to be less than 20%, except again for events with backward jets, where the reduction of the cross section due to fragmentation exceeds 20% and is again largest ($\sim 50\%$) when both jets have $\eta^{jet} < 0$.

Since the effect of fragmentation on the cross section depends on the Monte Carlo model, no attempt was made to correct the data for these effects. Instead, the effect of fragmentation is considered as a theoretical uncertainty.

5 Energy corrections

Kinematic variables are reconstructed using a combination of track and calorimeter information that optimises the resolution of reconstructed kinematic variables [34]. The selected calorimeter clusters and tracks are referred to as Energy Flow Objects (EFOs).

The use of track information reduces the sensitivity to energy losses in inactive material in front of the CAL. However, the energy of particles for which no track information is available (e.g. because the energy is deposited by a neutral particle), must be measured using CAL information. These energies have to be corrected for the energy losses in the inactive material. The conservation of energy and momentum in neutral-current deep inelastic scattering events is exploited to determine the required energy corrections [35] by balancing the scattered positron with the hadronic final state. This is done for data and Monte Carlo event samples independently. The EFOs thus corrected are used both for the reconstruction of jets and to determine kinematic variables. Comparisons between data and Monte Carlo of kinematic variables, reconstructed using corrected EFOs, lead to the assignment of a 3% correlated systematic uncertainty and a 2% uncorrelated systematic uncertainty in the transverse jet energies and in the hadronic variables [35].

6 Event selection

After applying the energy corrections described in Sect. 5, dijet events are selected from those events triggered by the dijet trigger [8] using the following procedures and cuts designed to remove sources of background:

- The k_T-clustering algorithm, in the inclusive mode with $R = 1$, is applied to the corrected EFOs. Events are selected in which at least two jets are found with: $-1 < \eta^{jet} < 2$, $E^{jet}_{T\,leading} > 14$ GeV and $E^{jet}_{T\,second} > 11$ GeV.
- To remove background due to proton beam-gas interactions and cosmic showers, a cut is made on the longitudinal position of the reconstructed interaction vertex

$$-40\,\text{cm} < Z_{vertex} < 40\,\text{cm}\,. \tag{4}$$

- To remove background due to charged-current deep inelastic scattering events, a cut is made on the relative missing transverse momentum:

$$\frac{P_T}{\sqrt{E_T}} < 1.5\sqrt{\text{GeV}}, \tag{5}$$

  where P_T and E_T are the transverse momentum and the transverse energy of the event, calculated on the basis of corrected EFOs.
- The rejection of neutral-current deep inelastic scattering (NC-DIS) events is based on the variable y. If a scattered positron candidate with energy greater than 5 GeV is found in the calorimeter, y can be calculated from the energy E'_e and the polar angle θ'_e of this positron candidate using the formula: $y_{elec} = 1 - \frac{E'_e}{2E_e}(1 - \cos\theta'_e)$. These events are rejected when:

$$y_{elec} < 0.7\,. \tag{6}$$

  The variable y can also be reconstructed from the observed hadronic final state using the Jacquet-Blondel formula [36]: $y_{JB} = \sum(E - p_z)/2E_e$, where the sum runs over all corrected EFOs. For all events it is required that

$$0.20 < y_{JB} < 0.85\,. \tag{7}$$

  This cut removes unidentified NC-DIS events, for which y_{JB} peaks at 1, and proton beam-gas interactions, which mostly have low y_{JB} values. The cuts on y_{elec} and y_{JB} effectively restrict the range of the virtuality of the exchanged photon to $Q^2 < 1$ GeV^2, with a median of about 10^{-3} GeV^2.

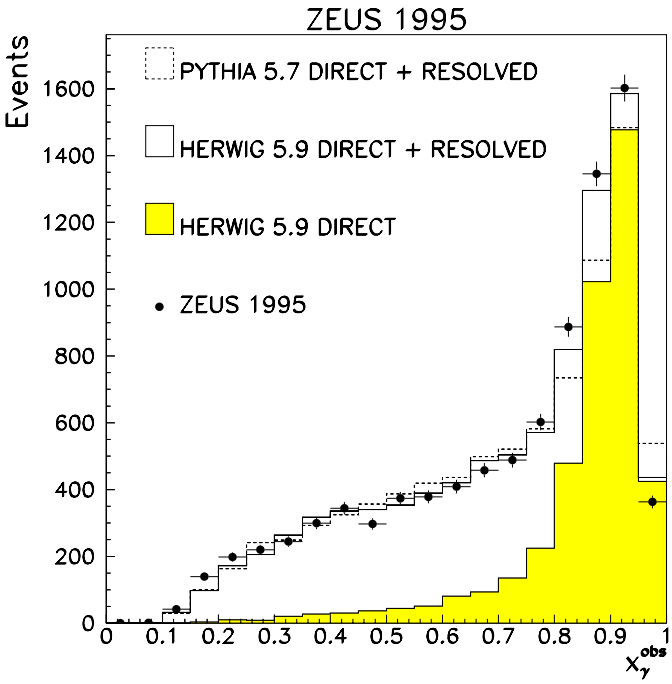

Fig. 1. The x_γ^{obs} spectrum of the selected dijet sample, compared to the HERWIG 5.9 and the PYTHIA 5.7 Monte Carlo predictions, which have been weighted as described in Sect. 7. The direct component from the HERWIG Monte Carlo is shown separately as the shaded histogram. Only statistical uncertainties are plotted

After the application of the described selection criteria, a sample of 8690 events remain. The contamination of this sample due to background processes was found to be negligible.

7 Event characteristics

Photoproduction events, generated using Monte Carlo programs, are used for the determination of acceptance and migration corrections and for the study of systematic uncertainties. These events are passed through a full simula-

tion of the ZEUS detector and undergo the same energy-correction procedure as the data.

Two leading-order Monte Carlo programs were used to generate dijet photoproduction events, HERWIG 5.9 [37, 38] and PYTHIA 5.7 [39,40]. Both models use leading-order matrix elements, but they differ in the treatment of parton showers, hadronisation and the virtuality spectrum of the exchanged photon. No additional process that would produce soft or hard underlying events is included in the simulations.

Direct and resolved event samples are generated separately. The parton density functions used to generate both Monte Carlo samples are CTEQ3-LO [41] for the proton and GRV-LO [30,31] for the photon.

As the Monte Carlo models do not include higher order matrix elements, they are not expected to describe the absolute normalisation of the cross section. To obtain the best agreement between data and Monte Carlo, the normalisation of the direct and resolved contributions is determined from a fit to the measured x_γ^{obs} spectrum. As a result the direct contribution of the HERWIG Monte Carlo is scaled by a factor 1.83 and the resolved contribution by a factor 1.72. For PYTHIA the direct contribution is scaled by 1.28 and the resolved contribution by 1.27. When these factors are applied, both Monte Carlo models are found to give a reasonable description of various distributions, such as the η^{jet} and E_T^{jet} spectra.

The x_γ^{obs} spectrum for the selected sample of the 8690 dijet events is shown in Fig. 1, where x_γ^{obs} is determined on the basis of corrected EFOs. The data show a clear peak near $x_\gamma^{obs} \sim 1$, attributed, at leading order to a predominance of "direct" events, and a tail towards low x_γ^{obs} values, attributed to "resolved" events. The data are compared to the HERWIG and PYTHIA Monte Carlo predictions, including the normalisation factors given above. The direct component of the HERWIG Monte Carlo is shown separately. The direct photoproduction events peak at high x_γ^{obs} values. Therefore, selecting events with $x_\gamma^{obs} > 0.75$ yields a sample strongly enriched with direct photoproduction events. After application of the normalisation factors described above, the Monte Carlo predictions are in good agreement with the data. The shape of the peak at high x_γ^{obs} is best described by the HERWIG Monte Carlo. Given the agreement in this distribution and in distributions like the η^{jet} and E_T^{jet} spectra (not shown here), the HERWIG Monte Carlo sample is used to determine acceptance and migration corrections and to study systematic uncertainties.

In Fig. 2 the transverse energy flow around jets is shown as a function of the distance in pseudorapidity $\Delta\eta$, with respect to the jet axis, integrated over $\Delta\phi$, between $\phi^{jet}-1$ and $\phi^{jet}+1$, where ϕ is measured in radians. The transverse energy flows are shown in bins of E_T^{jet} and x_γ^{obs}. The jets are strongly collimated, with relatively little transverse energy away from the jets. Comparison to the HERWIG predictions shows generally good agreement. Only at low x_γ^{obs} values is the energy flow outside the jet underestimated by the Monte Carlo model. Jets in the Monte Carlo are also found to be slightly narrower than jets in the data.

In the kinematic regime of the present analysis, Monte Carlo models that do not include a simulation of underlying events are able to describe the x_γ^{obs} distribution and the transverse energy flows, the only exception being the transverse energy flows in the lowest x_γ^{obs} bins, where a small discrepancy is observed. As these distributions are considered to be particularly sensitive to underlying events, this indicates that such processes play no role in the present kinematic regime. This result is different from what was observed in previous photoproduction analyses [5–9], in which jets at lower transverse energies were studied, where it was shown that the description of the data is improved when a model simulating soft or hard underlying events is included in the simulations.

8 Unfolding and systematics

The unfolding of the cross section is done by multiplying the number of events reconstructed in each bin by a correction factor determined from the HERWIG Monte Carlo sample. This correction factor is defined as the ratio of the number of events generated in the bin, N_{true}, over N_{rec}, the number of events reconstructed in the bin. The systematic uncertainty related to the choice of Monte Carlo model for the unfolding is estimated by using a different Monte Carlo generator, PYTHIA, to determine the correction factors. The HERWIG and PYTHIA Monte Carlo models differ in the treatment of the generation of the photon spectrum, the parton showers and the simulation of hadronisation effects. Nevertheless, both Monte Carlo models give a reasonable description of the data.

To determine systematic uncertainties in the measured cross sections, several variations in the event selection have been studied. The uncertainty in the cross section due to the energy-scale uncertainty is estimated by raising and lowering all energies in the Monte Carlo simulation by 3% simultaneously. In addition y and the transverse jet energies are varied by $\pm 2\%$ separately.

The systematic uncertainty related to the energy measurement is correlated from bin to bin. In the cross section figures presented in the next section, this uncertainty is shown separately. All other positive (negative) contributions to the cross section, from systematic uncertainties, are added in quadrature to yield the total positive (negative) systematic uncertainty.

9 Results

The dijet photoproduction cross section is presented as a function of three variables: $E_{T\,leading}^{jet}$, the transverse energy of the leading jet, and η_1^{jet} and η_2^{jet}, the pseudorapidities of the two jets. Statistical and systematic uncertainties, added in quadrature, are shown as thin error bars. Statistical uncertainties alone are shown as thick error bars and the uncertainty due to the energy scale is shown as a shaded band.

Table 1. The dijet cross section for the full x_γ^{obs} range and $0.20 < y < 0.85$, as a function of $E_{T\,leading}^{jet}$ in bins of the jet pseudorapidities

$d\sigma/dE_{T\,leading}^{jet}$ for: $0.20 < y < 0.85$ and all x_γ^{obs} values				
$E_{T\,leading}^{jet}$ GeV	$\mathrm{d}\sigma/\mathrm{d}E_{T\,leading}^{jet}$ pb/GeV	Δ_{stat} pb/GeV	Δ_{syst} (+/−) pb/GeV	$\Delta_{E-scale}$ (+/−) pb/GeV
$-1 < \eta_1^{jet} < 0$ & $-1 < \eta_2^{jet} < 0$				
14.0–17.0	13.6	1.2	0.9/ -2.2	3.2/ -1.2
17.0–21.0	1.81	0.37	1.16/ -0.54	0.60/ -0.26
$0 < \eta_1^{jet} < 1$ & $-1 < \eta_2^{jet} < 0$				
14.0–17.0	46.2	1.7	4.4/ -8.9	4.1/ -2.1
17.0–21.0	18.3	0.9	0.7/ -3.1	2.7/ -1.5
21.0–25.0	4.4	0.4	0.6/ -0.2	0.8/ -0.5
25.0–29.0	0.97	0.20	0.29/ -0.29	0.32/ -0.15
29.0–35.0	0.093	0.046	0.030/-0.063	0.035/-0.023
$1 < \eta_1^{jet} < 2$ & $-1 < \eta_2^{jet} < 0$				
14.0–17.0	41.2	1.6	2.4/ -7.1	5.8/ -1.0
17.0–21.0	16.9	0.8	0.5/ -1.4	1.2/ -1.2
21.0–25.0	5.1	0.5	0.7/ -0.4	0.7/ -0.6
25.0–29.0	1.56	0.26	0.17/ -0.23	0.29/ -0.19
29.0–35.0	0.42	0.11	0.24/ -0.05	0.10/ -0.08
$0 < \eta_1^{jet} < 1$ & $0 < \eta_2^{jet} < 1$				
14.0–17.0	81.8	3.0	3.1/ -1.8	11.9/ -1.6
17.0–21.0	42.5	1.9	0.5/ -4.8	4.1/ -2.6
21.0–25.0	18.2	1.2	2.4/ -2.5	2.6/ -1.1
25.0–29.0	7.5	0.8	0.3/ -0.7	1.1/ -0.8
29.0–35.0	2.4	0.4	0.1/ -0.3	0.3/ -0.3
35.0–41.0	0.49	0.16	0.14/ -0.04	0.12/ -0.05
$1 < \eta_1^{jet} < 2$ & $0 < \eta_2^{jet} < 1$				
14.0–17.0	73.7	2.0	1.7/ -3.0	9.0/ -0.5
17.0–21.0	40.4	1.3	0.7/ -2.6	4.7/ -2.9
21.0–25.0	17.9	0.9	0.2/ -1.3	1.9/ -1.6
25.0–29.0	8.2	0.6	0.1/ -1.0	1.1/ -1.0
29.0–35.0	2.8	0.3	0.7/ -0.6	0.4/ -0.4
35.0–41.0	1.18	0.18	0.25/ -0.41	0.13/ -0.14
41.0–48.0	0.20	0.07	0.15/ -0.03	0.04/ -0.02
48.0–55.0	0.28	0.10	0.04/ -0.19	0.06/ -0.05
$1 < \eta_1^{jet} < 2$ & $1 < \eta_2^{jet} < 2$				
14.0–17.0	49.6	2.3	4.0/ -2.0	7.1/ -0.8
17.0–21.0	30.4	1.6	1.0/ -2.9	3.4/ -2.7
21.0–25.0	15.0	1.1	0.5/ -1.9	1.6/ -1.5
25.0–29.0	6.2	0.7	0.7/ -0.7	0.8/ -0.6
29.0–35.0	2.8	0.4	0.3/ -0.3	0.3/ -0.4
35.0–41.0	1.53	0.29	0.05/ -0.60	0.25/ -0.12
41.0–48.0	0.39	0.14	0.05/ -0.06	0.06/ -0.07
48.0–55.0	0.099	0.070	0.183/-0.009	0.009/-0.007

Table 2. The dijet cross section for $x_\gamma^{obs} > 0.75$ and $0.20 < y < 0.85$, as a function of $E_{T\,leading}^{jet}$ in bins of the jet pseudorapidities

$d\sigma/dE_{T\,leading}^{jet}$ for: $0.20 < y < 0.85$ and $x_\gamma^{obs} > 0.75$				
$E_{T\,leading}^{jet}$ GeV	$\mathrm{d}\sigma/\mathrm{d}E_{T\,leading}^{jet}$ pb/GeV	Δ_{stat} pb/GeV	Δ_{syst} (+/−) pb/GeV	$\Delta_{E-scale}$ (+/−) pb/GeV
$-1 < \eta_1^{jet} < 0$ & $-1 < \eta_2^{jet} < 0$				
14.0–17.0	12.4	1.2	1.0/ -2.0	2.9/ -1.1
17.0–21.0	1.74	0.36	1.12/ -0.52	0.58/ -0.25
$0 < \eta_1^{jet} < 1$ & $-1 < \eta_2^{jet} < 0$				
14.0–17.0	37.1	1.5	3.5/ -7.7	3.3/ -1.7
17.0–21.0	15.4	0.8	1.1/ -2.5	2.3/ -1.3
21.0–25.0	4.2	0.4	0.5/ -0.2	0.8/ -0.5
25.0–29.0	0.93	0.19	0.22/ -0.32	0.30/ -0.14
29.0–35.0	0.093	0.046	0.030/-0.063	0.035/-0.023
$1 < \eta_1^{jet} < 2$ & $-1 < \eta_2^{jet} < 0$				
14.0–17.0	26.2	1.2	3.2/ -5.9	3.7/ -0.7
17.0–21.0	11.8	0.7	0.7/ -1.1	0.9/ -0.9
21.0–25.0	4.1	0.4	0.6/ -0.5	0.6/ -0.5
25.0–29.0	1.48	0.25	0.13/ -0.22	0.27/ -0.18
29.0–35.0	0.39	0.11	0.20/ -0.02	0.10/ -0.07
$0 < \eta_1^{jet} < 1$ & $0 < \eta_2^{jet} < 1$				
14.0–17.0	48.6	2.3	4.4/ -2.1	7.1/ -0.9
17.0–21.0	27.8	1.5	1.6/ -3.5	2.7/ -1.7
21.0–25.0	13.2	1.0	2.1/ -2.0	1.9/ -0.8
25.0–29.0	6.1	0.7	0.1/ -1.0	0.9/ -0.7
29.0–35.0	1.9	0.3	0.2/ -0.3	0.2/ -0.3
35.0–41.0	0.49	0.16	0.11/ -0.10	0.12/ -0.05
$1 < \eta_1^{jet} < 2$ & $0 < \eta_2^{jet} < 1$				
14.0–17.0	29.0	1.3	1.1/ -3.4	3.6/ -0.2
17.0–21.0	18.4	0.9	1.6/ -1.9	2.1/ -1.3
21.0–25.0	8.7	0.6	0.6/ -0.7	0.9/ -0.8
25.0–29.0	5.1	0.4	0.1/ -0.8	0.7/ -0.6
29.0–35.0	1.85	0.23	0.39/ -0.35	0.30/ -0.26
35.0–41.0	0.83	0.15	0.30/ -0.32	0.09/ -0.10
41.0–48.0	0.125	0.056	0.092/-0.012	0.023/-0.012
48.0–55.0	0.21	0.09	0.06/ -0.16	0.05/ -0.04
$1 < \eta_1^{jet} < 2$ & $1 < \eta_2^{jet} < 2$				
14.0–17.0	1.28	0.37	1.32/ -0.73	0.18/ -0.02
17.0–21.0	4.2	0.6	0.6/ -1.2	0.5/ -0.4
21.0–25.0	4.1	0.6	0.3/ -0.5	0.4/ -0.4
25.0–29.0	2.8	0.5	0.3/ -0.5	0.4/ -0.3
29.0–35.0	1.29	0.28	0.38/ -0.21	0.16/ -0.16
35.0–41.0	0.91	0.23	0.05/ -0.32	0.15/ -0.07
41.0–48.0	0.24	0.11	0.07/ -0.06	0.04/ -0.04
48.0–55.0	0.099	0.070	0.096/-0.009	0.009/-0.007

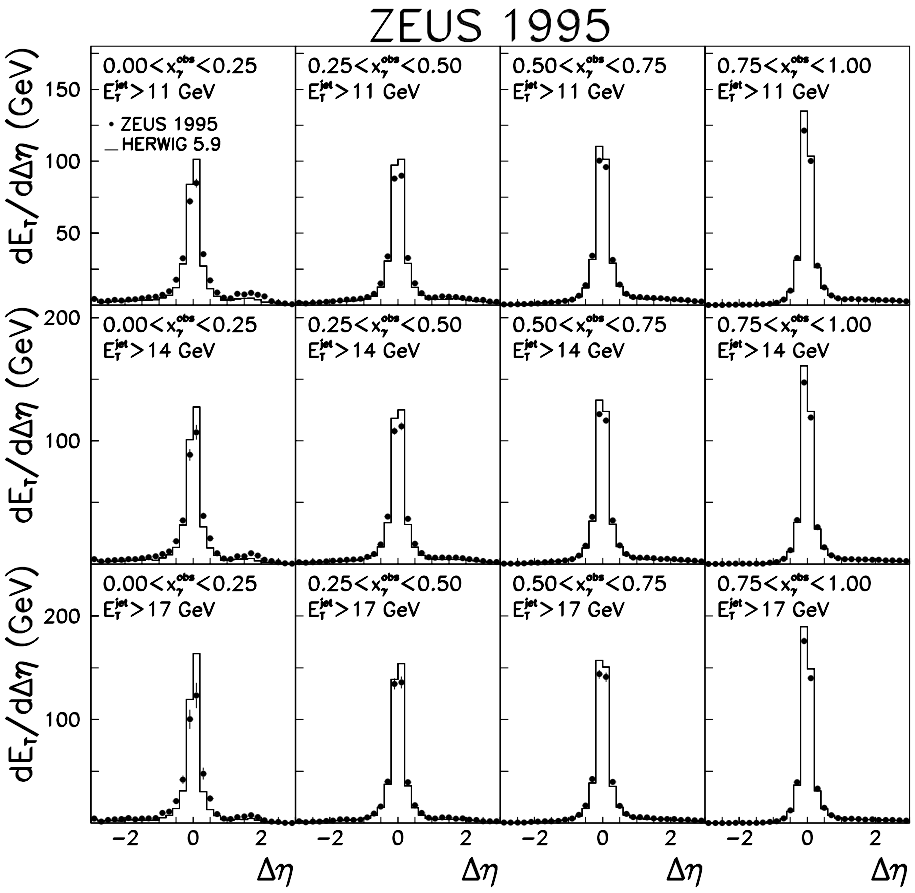

Fig. 2. The transverse energy flow around the jet axis (integrated over $|\Delta\phi| < 1$), in three ranges of the transverse energy of the jet and in four bins in x_γ^{obs}. The data are compared to the HERWIG 5.9 predictions. For the data only statistical uncertainties are shown

9.1 Cross sections for $134 < W_{\gamma p} < 277$ GeV

The dijet cross section as a function of the transverse energy of the leading jet is presented for six different ranges in jet pseudorapidity. These cross sections have been determined both for the full x_γ^{obs} range and for $x_\gamma^{obs} > 0.75$. Numerical values for the cross sections and the uncertainties are given in Table 1 and 2. The results are plotted in Fig. 3 and 4. The dijet cross section falls rapidly with increasing transverse energy of the leading jet. The steepest slopes occur when both jets are in the most backward pseudorapidity bin, $-1 < \eta_{1,2}^{jet} < 0$. High x_γ^{obs} events dominate the cross section at backward angles of the jets and at high transverse energies of the jets. This behaviour is expected on kinematic grounds, since high x_γ^{obs} values give access to the highest transverse jet energies and to the most backward pseudorapidities.

The data are compared to NLO-QCD calculations (see Sect. 4). Since the calculations from different groups are very similar, as will be shown in Fig. 5 and 6, only one set of calculations is shown here. This set corresponds to the GRV-HO [30,31] parameterisation of the photon structure, which gives the highest cross section. In general, the slopes and the absolute cross section are well described by the NLO-QCD calculations. However for events with forward jets, $1 < \eta_{1,2}^{jet} < 2$, and $E_{T\,leading}^{jet} < 25$ GeV the data lie above the predictions (see Fig. 3) and for events with very backward jets, $-1 < \eta_{1,2}^{jet} < 0$, the measurement lies below the calculations (see Fig. 4). The Monte Carlo studies discussed in Sect. 4 show that fragmentation decreases the measured cross section for events with negative pseudorapidities. It is therefore to be expected that the NLO-QCD calculations, in which no parton-to-hadron fragmentation is included, predict a higher cross section than that observed in this region.

The dijet cross section is also presented as a function of the pseudorapidity of one of the jets while keeping the other jet fixed in specific pseudorapidity ranges. Numerical values for the cross section and the uncertainties are given in Table 3 and 4 and are plotted in Fig. 5. The cross section peaks for events with η_2^{jet} near 1 and falls rapidly for events with $\eta_2^{jet} < 0$. The measurements are again compared to NLO-QCD calculations, but now using three different parameterisations for the parton densities in the photon. For the full x_γ^{obs} range, at central and forward pseudorapidities of the jets, the data lie above all predictions. At backward pseudorapidities, as was the case for the cross section as a function of $E_{T\,leading}^{jet}$, the data lie below the calculations. In the high x_γ^{obs} region, general agreement is seen between the data and the predictions.

Figure 5d shows a comparison between the NLO-QCD results from four different groups for the range $0 < \eta_1^{jet} < 1$. Each calculation uses the same parton density distributions for the proton, CTEQ4M [29], and the photon, GRV-HO [30,31]. The calculations from Aurenche et al.,

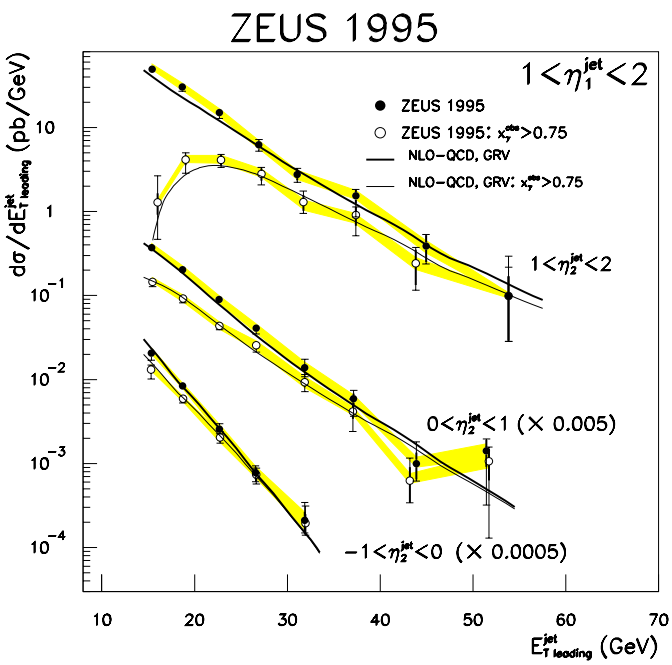

Fig. 3. Dijet cross section as a function of $E^{jet}_{T\,leading}$ for η^{jet}_1 between 1 and 2, in three regions of η^{jet}_2. The results for $-1 < \eta^{jet}_2 < 0$ and $0 < \eta^{jet}_2 < 1$ are scaled by the factors indicated in the figure. The filled circles correspond to the entire x^{obs}_γ range while the open circles correspond to events with $x^{obs}_\gamma > 0.75$. The shaded band indicates the uncertainty related to the energy scale. The thick error bar indicates the statistical uncertainty and the thin error bar indicates the systematic and statistical uncertainties added in quadrature. The data are compared to NLO-QCD calculations, using the GRV-HO parameterisation for the photon structure

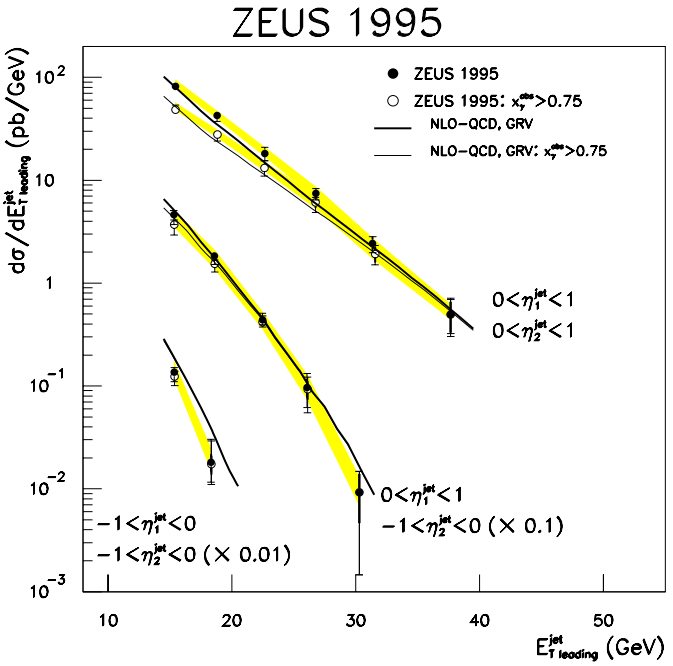

Fig. 4. Dijet cross section as a function of $E^{jet}_{T\,leading}$. For the two upper sets of data, η^{jet}_1 lies between 0 and 1 and for the lower set of data, η^{jet}_1 lies between -1 and 0. The η^{jet}_2 regions are indicated in the figure. The two lower sets of data are scaled by the factors indicated in the figure. The filled circles correspond to the entire x^{obs}_γ range while the open circles correspond to events with $x^{obs}_\gamma > 0.75$. The shaded band indicates the uncertainty related to the energy scale. The thick error bar indicates the statistical uncertainty and the thin error bar indicates the systematic and statistical uncertainties added in quadrature. The data are compared to NLO-QCD calculations, using the GRV-HO parameterisation for the photon structure

Frixione et al., Harris et al. and Klasen et al. agree to within a few percent.

In summary, it has been shown that NLO-QCD calculations generally describe the measured cross sections. However, for backward pseudorapidities the data are below the calculations, which is expected due to fragmentation, while for forward and central pseudorapidities the data are above the NLO predictions. In the latter kinematic region theoretical uncertainties are expected to be small.

9.2 Cross sections for $212 < W_{\gamma p} < 277$ GeV

The pseudorapidity dependence of the cross section has also been determined for events in a narrower region in y, which corresponds to a narrower range in $W_{\gamma p}$, the photon-proton CM energy. In such a region the sensitivity to the photon structure is expected to be larger. This follows from the relation between y, x^{obs}_γ and the pseudorapidities of the jets (see formula 2). Using a narrower range of y values implies that the cross section for specific pseudorapidities of the jets corresponds to a narrower range of x^{obs}_γ values. It is natural to select a narrow region of high y values rather than a narrow region of low y values, since, in the latter case, events with low x^{obs}_γ would fall out of the range of jet pseudorapidities, $-1 < \eta^{jet} < 2$.

Using a range of $0.50 < y < 0.85$, the cross section is presented as a function of the pseudorapidity of one of the jets while keeping the other jet fixed in a specific pseudorapidity bin. Values for the cross section and the uncertainties are given in Table 5 and 6 and are shown in Fig. 6. The cross section for this high-y region peaks at more backward pseudorapidities than the cross section for the full y range, as observed in a previous ZEUS study [9], and also the peak is more pronounced than for the full y range. This observation is consistent with the expected closer correlation between η^{jets} and x^{obs}_γ when the y range is restricted. The peak in the cross sections at backward pseudorapidities reflects the peak near $x^{obs}_\gamma \sim 1$ in Fig. 1 and the tail towards positive pseudorapidities corresponds to low x^{obs}_γ values.

The measurements are again compared to NLO-QCD calculations using the GRV-HO, AFG-HO and GS96-HO parameterisations of the photon structure. The NLO pre-

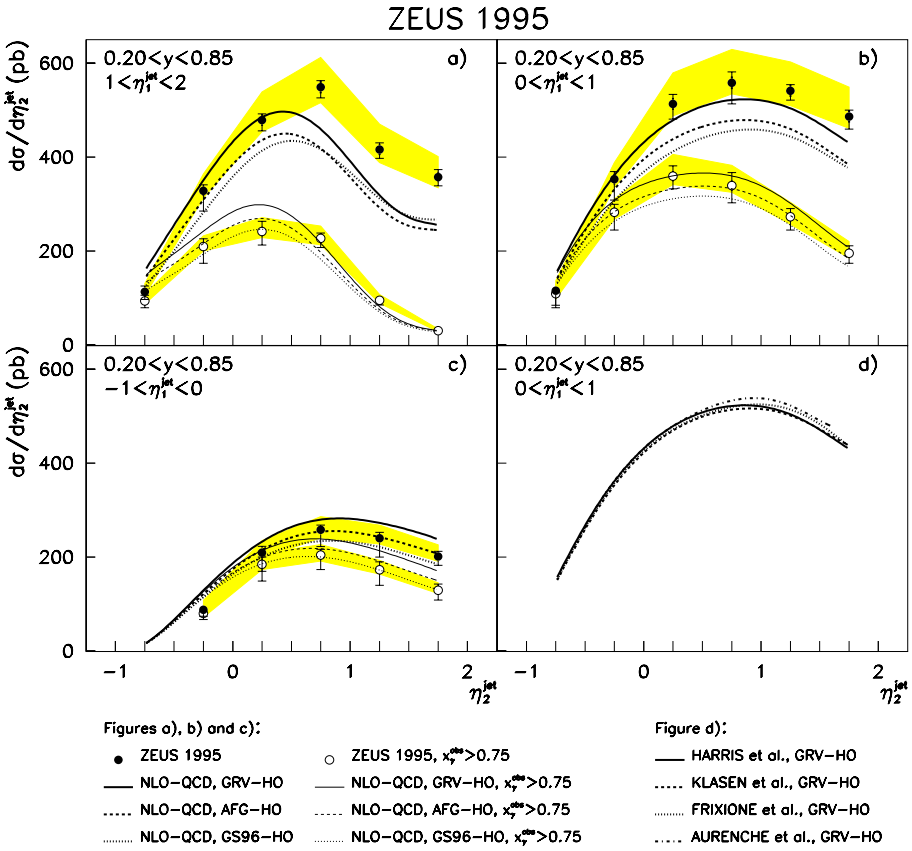

Fig. 5. a–c show the dijet cross section as a function of η_2^{jet} in bins of η_1^{jet}. The filled circles correspond to the entire x_γ^{obs} range while the open circles correspond to events with $x_\gamma^{obs} > 0.75$. The shaded band indicates the uncertainty related to the energy scale. The thick error bar indicates the statistical uncertainty and the thin error bar indicates the systematic and statistical uncertainties added in quadrature. The full, dotted and dashed curves correspond to NLO-QCD calculations, using the GRV-HO, GS96-HO and the AFG-HO parameterisations for the photon structure, respectively. In **d** the NLO-QCD results for the cross section when $0 < \eta_1^{jet} < 1$ and for a particular parameterisation of the photon structure are compared

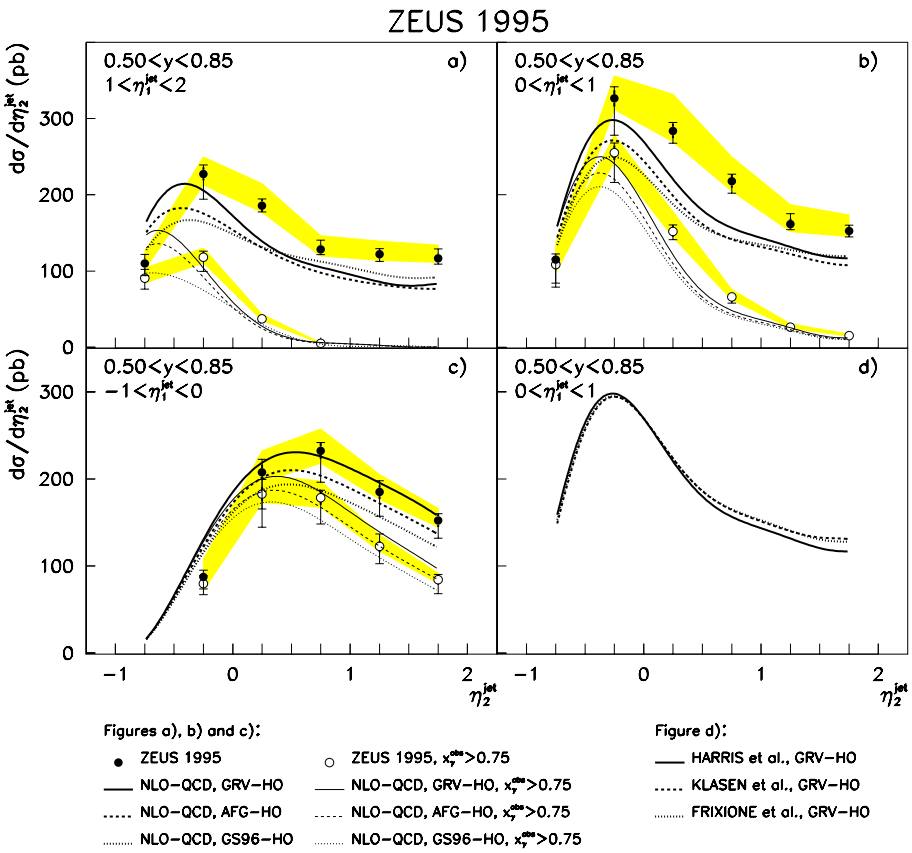

Fig. 6. a–c show the dijet cross section as a function of η_2^{jet} in bins of η_1^{jet} and for $0.50 < y < 0.85$. The filled circles correspond to the entire x_γ^{obs} range while the open circles correspond to events with $x_\gamma^{obs} > 0.75$. The shaded band indicates the uncertainty related to the energy scale. The thick error bar indicates the statistical uncertainty and the thin error bar indicates the systematic and statistical uncertainties added in quadrature. The full, dotted and dashed curves correspond to NLO-QCD calculations, using the GRV-HO, GS96-HO and the AFG-HO parameterisations for the photon structure, respectively. In **d** the NLO-QCD results for the cross section when $0 < \eta_1^{jet} < 1$ and for a particular parameterisation of the photon structure are compared

Table 3. The dijet cross section, for all x_γ^{obs} values and $0.20 < y < 0.85$, as a function of η_2^{jet}, for η_1^{jet} fixed

$d\sigma/d\eta^{jet}$ for: $0.20 < y < 0.85$ and all x_γ^{obs} values				
η_2^{jet}	$\mathrm{d}\sigma/\mathrm{d}\eta_2^{jet}$ pb	Δ_{stat} pb	Δ_{syst} (+/−) pb	$\Delta_{E-scale}$ (+/−) pb
$-1 < \eta_1^{jet} < 0$				
-0.5–0.0	88	5	6/ -13	20/ -9
0.0–0.5	209	9	10/ -39	26/ -13
0.5–1.0	258	9	4/ -34	28/ -17
1.0–1.5	240	9	9/ -39	28/ -12
1.5–2.0	201	8	7/ -17	25/ -10
$0 < \eta_1^{jet} < 1$				
-1.0—0.5	115	7	4/ -30	21/ -12
-0.5–0.0	353	11	11/ -44	35/ -19
0.0–0.5	513	13	16/ -29	66/ -25
0.5–1.0	558	14	19/ -43	71/ -23
1.0–1.5	541	13	1/ -15	61/ -32
1.5–2.0	486	13	6/ -23	63/ -25
$1 < \eta_1^{jet} < 2$				
-1.0—0.5	113	6	10/ -15	18/ -8
-0.5–0.0	328	11	7/ -42	36/ -15
0.0–0.5	479	12	4/ -19	60/ -25
0.5–1.0	549	14	1/ -18	63/ -33
1.0–1.5	416	12	9/ -14	54/ -28
1.5–2.0	358	11	12/ -15	43/ -23

Table 4. The dijet cross section for $x_\gamma^{obs} > 0.75$ and $0.20 < y < 0.85$, as a function of η_2^{jet}, for η_1^{jet} fixed

$d\sigma/d\eta^{jet}$ for: $0.20 < y < 0.85$ and $x_\gamma^{obs} > 0.75$				
η_2^{jet}	$\mathrm{d}\sigma/\mathrm{d}\eta_2^{jet}$ pb	Δ_{stat} pb	Δ_{syst} (+/−) pb	$\Delta_{E-scale}$ (+/−) pb
$-1 < \eta_1^{jet} < 0$				
-0.5–0.0	80	5	8/ -12	18/ -8
0.0–0.5	185	8	13/ -35	23/ -11
0.5–1.0	204	8	9/ -30	23/ -13
1.0–1.5	173	8	15/ -32	20/ -9
1.5–2.0	129	7	12/ -19	16/ -7
$0 < \eta_1^{jet} < 1$				
-1.0—0.5	109	7	3/ -29	20/ -11
-0.5–0.0	283	10	14/ -37	28/ -15
0.0–0.5	359	11	19/ -25	46/ -18
0.5–1.0	339	11	26/ -35	43/ -14
1.0–1.5	273	9	15/ -27	31/ -16
1.5–2.0	195	8	14/ -20	25/ -10
$1 < \eta_1^{jet} < 2$				
-1.0—0.5	94	6	11/ -13	15/ -7
-0.5–0.0	210	8	14/ -35	23/ -9
0.0–0.5	241	9	20/ -27	30/ -12
0.5–1.0	227	9	7/ -18	26/ -14
1.0–1.5	95	6	6/ -8	12/ -6
1.5–2.0	30	3	2/ -2	4/ -2

dictions show an enhanced sensitivity to the choice of parameterisation for the photon structure. In particular in the region $1 < \eta_1^{jet} < 2$ there are clear differences in shape between the NLO predictions corresponding to different parton densities in the photon. In the most backward bins, where $\eta_2^{jet} < -0.5$ or where $\eta_{1,2}^{jet} < 0$, the data again lie below the calculations, but, as stated above, fragmentation effects are large in this region. At central and forward pseudorapidities, both for the full and for the high x_γ^{obs} range, the data lie above the NLO calculations.

In Fig. 6d a comparison is again made between the NLO-QCD results from different groups. The calculations agree to within a few percent.

The fact that the cross sections, measured in the region where jets are produced at central and forward pseudorapidities and where theoretical uncertainties are expected to be small, lie above the NLO-QCD predictions, suggests that in this kinematic region the parton densities in the photon are too small in the available parameterisations. The disagreement between the data and the calculations is observed for the full x_γ^{obs} range and to a lesser extent also for $x_\gamma^{obs} > 0.75$. It is strongest at central pseudorapidities. This region corresponds to values of x_γ that lie roughly between 0.5 and 1.

10 Summary and conclusions

A measurement of dijet photoproduction, in the range $0.20 < y < 0.85$, $Q^2 < 1\,\mathrm{GeV}^2$, $-1 < \eta^{jet} < 2$, $E_{T\,leading}^{jet} > 14$ GeV and $E_{T\,second}^{jet} > 11$ GeV, has been presented. Jets are defined in the hadronic final state by applying the k_T-clustering jet algorithm. The cross section has been compared to NLO-QCD predictions.

For the full y region, $0.20 < y < 0.85$, corresponding to $134 < W_{\gamma p} < 277$ GeV, the dijet cross section has been measured as a function of the transverse energy of the leading jet and as a function of the pseudorapidities of the jets. The dependence on the transverse energy of the leading jet is generally well described by the NLO-QCD calculations, although for events with two forward-going jets and $E_{T\,leading}^{jet} < 25$ GeV, the data lie above the NLO-QCD calculations. Also, the cross section as a function of the pseudorapidities of the jets lies above the NLO-QCD calculations at central and forward pseudorapidities. In the region $x_\gamma^{obs} > 0.75$, the calculations agree with the measured cross section.

In the high-y region, $0.50 < y < 0.85$ ($212 < W_{\gamma p} < 277$ GeV), where a stronger sensitivity to the photon structure is expected, the cross section at central and forward pseudorapidities lies further above the predictions than

Table 5. The dijet cross section, for all x_γ^{obs} values and $0.50 < y < 0.85$, as a function of η_2^{jet}, for η_1^{jet} fixed

$d\sigma/d\eta^{jet}$ for: $0.50 < y < 0.85$ and all x_γ^{obs} values				
η_2^{jet}	$\mathrm{d}\sigma/\mathrm{d}\eta_2^{jet}$ pb	Δ_{stat} pb	Δ_{syst} (+/−) pb	$\Delta_{E-scale}$ (+/−) pb
$-1 < \eta_1^{jet} < 0$				
-0.5–0.0	88	5	6/ -13	20/ -9
0.0–0.5	208	9	12/ -41	25/ -11
0.5–1.0	232	9	2/ -35	25/ -14
1.0–1.5	185	8	11/ -26	20/ -8
1.5–2.0	152	7	2/ -19	14/ -8
$0 < \eta_1^{jet} < 1$				
-1.0—0.5	115	7	4/ -30	21/ -12
-0.5–0.0	326	11	11/ -47	29/ -15
0.0–0.5	284	10	6/ -13	48/ -14
0.5–1.0	218	9	3/ -13	32/ -13
1.0–1.5	162	7	12/ -2	26/ -10
1.5–2.0	153	7	3/ -3	21/ -8
$1 < \eta_1^{jet} < 2$				
-1.0—0.5	110	6	10/ -15	16/ -8
-0.5–0.0	227	9	8/ -32	22/ -14
0.0–0.5	186	8	4/ -4	29/ -9
0.5–1.0	128	6	11/ -3	18/ -8
1.0–1.5	122	6	4/ -7	17/ -8
1.5–2.0	117	6	11/ -5	17/ -5

Table 6. The dijet cross section for $x_\gamma^{obs} > 0.75$ and $0.50 < y < 0.85$, as a function of η_2^{jet}, for η_1^{jet} fixed

$d\sigma/d\eta^{jet}$ for: $0.50 < y < 0.85$ and $x_\gamma^{obs} > 0.75$				
η_2^{jet}	$\mathrm{d}\sigma/\mathrm{d}\eta_2^{jet}$ pb	Δ_{stat} pb	Δ_{syst} (+/−) pb	$\Delta_{E-scale}$ (+/−) pb
$-1 < \eta_1^{jet} < 0$				
-0.5–0.0	80	5	8/ -12	18/ -8
0.0–0.5	183	8	15/ -37	22/ -10
0.5–1.0	178	8	4/ -29	19/ -11
1.0–1.5	122	6	13/ -18	13/ -5
1.5–2.0	84	5	3/ -15	8/ -4
$0 < \eta_1^{jet} < 1$				
-1.0—0.5	108	7	4/ -29	20/ -11
-0.5–0.0	255	9	9/ -38	23/ -12
0.0–0.5	152	7	5/ -9	26/ -8
0.5–1.0	66	5	0/ -7	10/ -4
1.0–1.5	27	3	2/ -1	4/ -2
1.5–2.0	15	2	2/ -1	2/ -1
$1 < \eta_1^{jet} < 2$				
-1.0—0.5	91	6	10/ -13	13/ -6
-0.5–0.0	118	6	5/ -18	12/ -7
0.0–0.5	37	3	0/ -4	6/ -2
0.5–1.0	5.0	1.2	2.5/ -0.5	0.7/ -0.3

for the full y range. Also the cross section lies above the NLO-QCD calculations for $x_\gamma^{obs} > 0.75$.

Since theoretical uncertainties are expected to be small in most of the kinematic regime of the present analysis, as was discussed in Sects. 4 and 7, the discrepancies observed between the data and the NLO-QCD calculations suggest that, in the kinematic region of the present analysis, the available parameterisations of the parton densities in the photon are too small.

The results presented in this paper cover a kinematic region where both x_γ^{obs} and E_T^{jet}, which acts as the factorisation scale, are high. This region has not been studied in F_2^γ measurements. It remains to be established whether the parton density functions in the photon can be modified to describe the present data while remaining consistent with the existing F_2^γ data from e^+e^- experiments. It is hoped that phenomenologists carrying out comprehensive NLO-QCD fits will be able to include the data in this paper in their fits to determine the parton density functions in the photon and thereby clarify this issue.

Acknowledgements. We thank the DESY Directorate for their strong support and encouragement. The remarkable achievements of the HERA machine group were essential for the successful completion of this work and are greatly appreciated. We would like to thank M. Fontannaz, S. Frixione, B. Harris and M. Klasen for providing us with their NLO calculations or code and for useful discussions on theoretical issues. This paper was completed shortly after the tragic and untimely death of Prof. Dr. B.H. Wiik, Chairman of the DESY directorate. All members of the ZEUS collaboration wish to acknowledge the remarkable role which he played in the success of both the HERA project and of the ZEUS experiment. His inspired scientific leadership, his warm personality and his friendship will be sorely missed by us all.

References

1. BCDMS Collaboration, A.C. Benvenuti et al., *Phys. Lett.* B **223**, 485 (1990); NMC Collaboration, M. Arneodo et al., *Nucl. Phys.* B **483**, 3 (1997); H1 Collaboration, S. Aid et al., *Nucl. Phys.* B **470**, 3 (1996); ZEUS Collaboration, M. Derrick et al., *Z. Phys.* C **72**, 399 (1996)
2. L3 Collaboration, M. Acciarri et al., *Phys. Lett.* B **436**, 403 (1998); L3 Collaboration, M. Acciarri et al., *Phys. Lett.* B **447**, 147 (1999); DELPHI Collaboration, P. Abreu et al., *Z. Phys.* C **69**, 223 (1996); OPAL Collaboration, K. Ackerstaff et al., *Phys. Lett.* B **412**, 225 (1997); OPAL Collaboration, K. Ackerstaff et al., *Phys. Lett.* B **411**, 387 (1997); OPAL Collaboration, K. Ackerstaff et al., *Z. Phys.* C **74**, 33 (1997); OPAL Collaboration, R. Akers et al., *Z. Phys.* C **61**, 199 (1994); TOPAZ Collaboration, K. Muramatsu et al., *Phys. Lett.* B **332**, 477 (1994); AMY Collaboration,

T. Kojima et al., *Phys. Lett.* B **400**, 395 (1997); AMY Collaboration, S.K. Sahu et al., *Phys. Lett.* B **346**, 208 (1995); AMY Collaboration, T. Sasaki et al., *Phys. Lett.* B **252**, 491 (1990); TPC/2γ Collaboration, H. Aihara et al., *Z. Phys.* C **34**, 1 (1987); TPC/2γ Collaboration, H. Aihara et al., *Phys. Rev. Lett.* **58**, 97 (1987); CELLO Collaboration, H.J. Behrend et al., *Phys. Lett.* B **126**, 391 (1983); JADE Collaboration, W. Bartel et al., *Z. Phys.* C **24**, 231 (1984); JADE Collaboration, W. Bartel et al., *Phys. Lett.* B **121**, 203 (1983); TASSO Collaboration, M. Althoff et al., *Z. Phys.* C **31**, 527 (1986); PLUTO Collaboration, Ch. Berger et al., *Nucl. Phys.* B **281**, 365 (1987); PLUTO Collaboration, Ch. Berger et al., *Phys. Lett.* B **142**, 111 (1984); PLUTO Collaboration, Ch. Berger et al., *Phys. Lett.* B **107**, 168 (1981)
3. DØ Collaboration, B. Abbott et al., *Phys. Rev. Lett.* **82**, 2451 (1999); CDF Collaboration, F. Abe et al., *Phys. Rev. Lett.* **77**, 438 (1996); CDF Collaboration, F. Abe et al., *Phys. Rev. Lett.* **70**, 1376 (1993)
4. J. Huston, hep-ph/9901352; G.C. Blazey and B.L. Flaugher, FERMILAB-PUB-99-038-E, submitted to *Ann. Rev. Nucl. Part. Sci.*
5. ZEUS Collaboration, M. Derrick et al., *Phys. Lett.* B **342**, 417 (1995)
6. ZEUS Collaboration, M. Derrick et al., *Phys. Lett.* B **348**, 665 (1995)
7. H1 Collaboration, S. Aid et al., *Z. Phys.* C **70**, 17 (1996)
8. ZEUS Collaboration, J. Breitweg et al., *Eur. Phys. J.* C **1**, 109 (1998)
9. ZEUS Collaboration, J. Breitweg et al., *Eur. Phys. J.* C **4**, 591 (1998)
10. ZEUS Collaboration, J. Breitweg et al., *Phys. Lett.* B **443**, 394 (1998)
11. M. Klasen, G. Kramer, S.G. Salesch, *Z. Phys.* C **68**, 113 (1995)
12. M. Klasen and G. Kramer, *Phys. Lett.* B **366**, 385 (1996)
13. S. Frixione and G. Ridolfi, *Nucl. Phys.* B **507**, 315 (1997)
14. W.T. Giele, E.W.N. Glover and D.A. Kosower, *Phys. Rev. Lett.* **73**, 2019 (1994)
15. S. Catani, Yu.L. Dokshitzer, M.H. Seymour and B.R. Webber, *Nucl. Phys.* B **406**, 187 (1993)
16. S.D. Ellis and D.E. Soper, *Phys. Rev.* D **48**, 3160 (1993)
17. M.H. Seymour, hep-ph/9707349; J.M. Butterworth, L. Feld, M. Klasen and G. Kramer, Proceedings of the Workshop "Future Physics at HERA", 554 (1996)
18. P. Aurenche, L. Bourhis, M. Fontannaz and J.Ph. Guillet, Proceedings of the Workshop "Future Physics at HERA", 570 (1996)
19. S. Frixione, *Nucl. Phys.* B **507**, 295 (1997)
20. B.W. Harris and J.F. Owens, *Phys. Rev.* D **56**, 4007 (1997)
21. M. Klasen and G. Kramer, *Z. Phys.* C **76**, 67 (1997); M. Klasen, T. Kleinwort and G. Kramer, *Eur. Phys. J.* C **1**, 1 (1998)
22. M. Klasen and G. Kramer, *Z. Phys.* C **72**, 107 (1996); L.J. Bergmann, Ph.D. Thesis, Florida State University, 1989
23. S. Frixione, Z. Kunszt and A. Signer, *Nucl. Phys.* B **467**, 399 (1996)
24. B.W. Harris and J.F. Owens, *Phys. Rev.* D **57**, 5555 (1998)
25. The ZEUS Detector, Status Report (1993), DESY 1993
26. ZEUS Collaboration, M. Derrick et al., *Nucl. Instrum. Methods* A **309**, 77 (1991)
27. A. Andresen et al., *Nucl. Instrum. Methods* A **309**, 101 (1991); A. Bernstein et al., *Nucl. Instrum. Methods* A **336**, 23 (1993)
28. N. Harnew et al., *Nucl. Instrum. Methods* A **279**, 290 (1989); B. Foster et al., *Proc. Suppl. Nucl. Phys.* B **32**, 181 (1993); B. Foster et al., *Nucl. Instrum. Methods* A **338**, 254 (1994)
29. H.L. Lai et al., *Phys. Rev.* D **55**, 1280 (1997)
30. M. Glück, E. Reya and A. Vogt, *Phys. Rev.* D **45**, 3986 (1992)
31. M. Glück, E. Reya and A. Vogt, *Phys. Rev.* D **46**, 1973 (1992)
32. L.E. Gordon and J.K. Storrow, *Nucl. Phys.* B **489**, 405 (1997)
33. P. Aurenche, J. Guillet and M. Fontannaz, *Z. Phys.* C **64**, 621 (1994)
34. G.M. Briskin, Ph.D. Thesis, Tel Aviv University, 1998 (unpublished)
35. J.H. Vossebeld, Ph.D. Thesis, University of Amsterdam, 1999 (unpublished)
36. F. Jacquet and A. Blondel, Proceedings of the study of an *ep* facility for Europe, DESY 79-048, 391 (1979)
37. G. Marchesini et al., *Comp. Phys. Commun.* **67**, 465 (1992)
38. G. Marchesini et al., hep-ph/9607393
39. H.U. Bengtsson and T. Sjöstrand, *Comp. Phys. Commun.* **46**, 43 (1987)
40. T. Sjöstrand, *Comp. Phys. Commun.* **82**, 74 (1994)
41. H.L. Lai et al., *Phys. Rev.* D **51**, 4763 (1995)